THE PENNSYLVANIA STATE UNIVERSITY
SCHREYER HONORS COLLEGE

DEPARTMENT OF MECHANICAL AND NUCLEAR ENGINEERING

VEHICLE TO VEHICLE COMPARISON OF TIRE AND CHASSIS DYNAMICS

Dennis J. Plank

Spring 2007

A thesis
submitted in partial fulfillment
of the requirements
for a baccalaureate degree
in Mechanical Engineering
with honors in Mechanical Engineering

Approved: ______________________________ Date: ______________________

Sean N. Brennan
Assistant Professor of Mechanical Engineering
Thesis Supervisor

______________________________ ______________________

Domenic A. Santavicca
Professor of Mechanical Engineering
Honors Adviser

______________________________ ______________________

Committee Member Name

______________________________ ______________________

Department/Program Head Name

ABSTRACT

In academia, vehicle dynamics is studied for several purposes, including the improvement of vehicle safety through control algorithms and the advancement of autonomous vehicle technology. Tire and chassis dynamic parameters are often required in the course of research, but no public database or simple, proven method of obtaining the parameters exists. This work focuses on the validation of a method that can obtain these tire and chassis parameters without the use of expensive specialized tire and chassis testing machines.

Also discussed is an instrumentation package that centers around a Global Position System (GPS) integrated with an Inertial Navigation System (INS). The construction and calibration of several steering angle sensors is presented.

For the mathematical analysis of the test data, a 2-DOF Bicycle Model is used. The assumptions and limitations of this model are fully discussed, as are how these factors may contribute to errors in the results.

The results of testing are compared to previous test results and a few sample parameter values obtained from other published works. Differences between the current data and the other data are explored and possible reasons for the differences are proposed.

Finally, the challenges of obtaining tire and chassis parameters are discussed and potential improvements to the testing method are suggested.

TABLE OF CONTENTS

List of Figures

ACKNOWLEDGEMENTS

First and foremost, I would like to thank Dr. Sean Brennan. Dr. Brennan has taught me, advised me, and inspired me. Without his tutelage and passion for vehicle and systems research, this thesis simply would not have been possible.

I would also like to thank all of the other students in the Intelligent Vehicles and Systems research group. While all of them have provided me with support and camaraderie during my research, Bridget Hamblin deserves special mention for her dedication to helping me for long hours at the test track and teaching me about vehicle theories and the testing systems.

And finally, I would like to thank my family and friends, who always help me as I reach for my dreams.

Chapter 1

Introduction

This thesis will focus on the validation of procedures used to obtain tire cornering stiffness through the testing of the vehicle as a whole. Also addressed will be the refinement, implementation, and calibration of a modular instrumentation system that can be used in conjunction with the procedure to efficiently capture data. The primary goal of this work is to advance the testing instruments and apply the procedure to another vehicle in order to confirm the consistency and accuracy of the method by comparing the present results to previous studies.

Motivation

Tires are the source of the forces that make vehicles change direction and speed. The lateral force production of a tire directly influences the handling of a vehicle. Handling, in turn, is related to subjective driver feel and more importantly, the performance capabilities of the vehicle. Because of its effect on vehicle handling, tire lateral force is a significant variable in vehicle dynamics.

Despite this significance, very little tire lateral force test data is available to the public. The inherent complexity of a tire, the wide variation in properties among different tires, and the high cost of tire testing machines all contribute to this knowledge deficit. Nationwide, only several organizations such as tire manufacturers and Calspan's

Tire Research Facility have the capability to measure tire lateral force. The MTS Flat-Trac machine, shown in Fig. **1.1**, is an example of a common type of tire testing apparatus, the belt-style machine [**2**]. However, the difficulty of obtaining tire test data remains a major challenge to those interested in vehicle dynamics [**1**].

Figure **1.1**: MTS Flat-Trac Tire Test Machine

Previous Work

The prior research and publications of Dr. Sean Brennan's Intelligent Vehicles and Systems Group at The Pennsylvania State University was instrumental in facilitating this thesis. In 2006, the group successfully integrated a Global Positioning System (GPS) and Inertial Navigation System (INS) in the interest of studying vehicle modeling and control, with an emphasis on improving vehicle safety [**3**][**4**]. As a component of this work, a method to obtain tire properties by using the GPS/INS system was developed on one vehicle. The instruments and methods used in those studies were similar to ones initially developed by David Bevly (currently of Auburn University) at Stanford University in 2001 [**5**]. The Stanford group also combined a GPS and INS system and developed methods to obtain vehicle and tire properties, although the actual hardware and testing procedures were much different. However, the work demonstrated that a GPS/INS system could be used to improve the accuracy of vehicle state measurements and provide estimates of tire properties. All of the aforementioned research relies on assumptions and simple tire and vehicle models presented in early vehicle dynamics works by L. Segel [**6**] and R.T. Bundorf [**7**] and in more recent textbooks such as by T.D. Gillespie [**8**]. Without these tools, the complexity of vehicle motion is too great for easy analysis. The remainder of this chapter will detail these assumptions and models.

Two Degree-of-Freedom Model

To better understand the specific nature and impact of tire forces, the two degree-of-freedom vehicle model commonly known as the Bicycle Model will be presented. Higher order models exist, and although the Bicycle Model is the most basic, it is still considered to be reasonably accurate and is frequently used to study vehicle dynamics. Higher order models are designed to account for complicated or high frequency vehicle movements that are assumed not to occur in the Bicycle Model [**9**]. Because the goal of this work is to find a simple way to obtain tire and vehicle properties, the Bicycle Model will be used because of its relative simplicity.

The model is known as the Bicycle Model because one of the primary assumptions is that the mass of the vehicle and the tire forces are symmetric about the X-Z plane, as defined in the Society of Automotive Engineers (SAE) body-fixed vehicle coordinate system shown in Fig. **1.2**. This assumption allows a vehicle with four wheels to be modeled as a two-wheeled vehicle, with each modeled wheel representing a two-wheeled axle on a real vehicle. Other primary assumptions are that velocity is constant in the longitudinal direction; that the tires do not slip in the longitudinal direction (there is no driving or braking occurring); that the effects of lateral roll are ignored; and that the tire force is linearly proportional to the tire side-slip angle. A final assumption is that all angles are small, so that $\cos(\theta) \approx 1$ and $\sin(\theta) \approx \theta$.

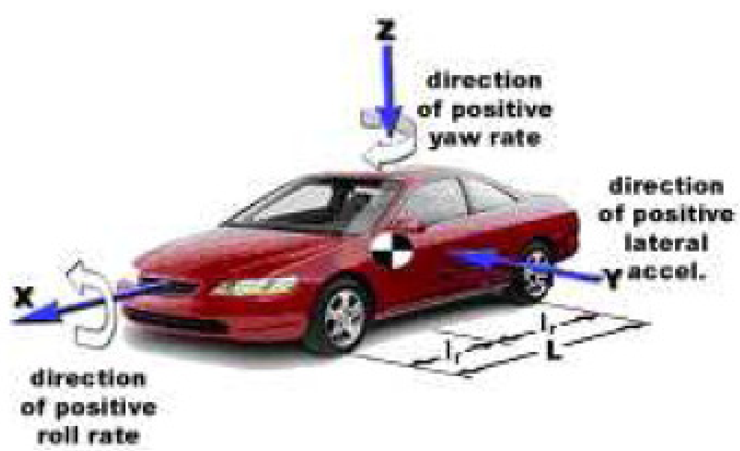

Figure **1.2**: SAE Vehicle Coordinate System

The states of the Bicycle Model are the lateral velocity and the yaw rate, measured at the center of gravity and about the Z-axis, respectively. Figure Fig. **1.3** shows a depiction of the model and Fig. **1.4** lists the model parameters.

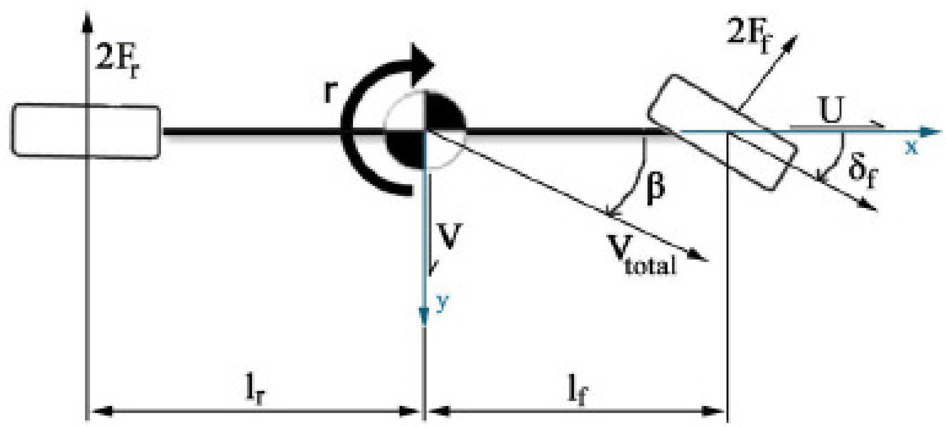

Figure **1.3**: The Bicycle Model

Parameter	Definition
U	Longitudinal velocity (body-fixed frame)
r	Yaw rate (angular rate about vertical axis)
m	Vehicle mass
I_{zz}	Inertia about the vertical axis
l_f	front-axle-to-CG distance
l_r	rear-axle-to-CG distance
L	Track of vehicle (lf + lr)
t	Width of vehicle
β	Slip angle of the vehicle body
C_f	Front cornering stiffness
C_r	Rear cornering stiffness
δ_f	Front steering angle

Figure **1.4**: Bicycle Model Parameters

The aforementioned tire slip angle is depicted in Fig. **1.5**. As shown in the figure, the slip angle α is defined as the angle between the tire's centerline and its velocity vector. The slip angle plays a large role in the derivation of the Bicycle Model force equations.

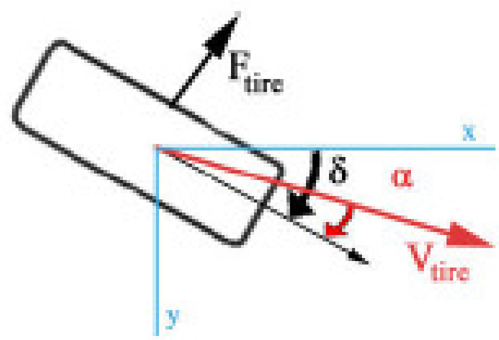

Figure **1.5**: Tire Velocity Vectors

Bicycle Model Equations

The constant that relates the tire slip angle to the lateral force produced by the tire is known as cornering stiffness and has units of *N/rad.* Typically, the front and rear cornering stiffnesses are labeled as C_f and C_r, respectively. In the SAE system, the cornering stiffness values are positive by convention. Eq. **1.1** shows the relationship between lateral force, slip angle, and cornering stiffness.

$$\begin{aligned} F_f &= C_f \alpha_f \\ F_r &= C_r \alpha_r \end{aligned} \qquad \text{Equation } \mathbf{1.1}$$

For a rigorous derivation of these equations, “A Primer on Vehicle Directional Control” by R.T. Bundorf or a number of vehicle dynamics textbooks may be consulted [**4**]. The final form of the Bicycle Model is shown in Eq. **1.2**, where R is the radius of the turn and W_f and W_r represent the front and rear vehicle axle weights. In this form, negative values of cornering stiffness must be used.

$$\delta_f = \frac{L}{R} + \left(\frac{W_r}{C_r} - \frac{W_f}{C_f} \right) \frac{U^2}{g \cdot R} \qquad \text{Equation } \mathbf{1.2}$$

An important parameter related to this equation is the understeer gradient. The understeer gradient quantifies the amount of steering input change necessary when varying the radius of curvature or speed at which a vehicle is traveling. The understeer gradient can be measure experimentally and can be used to find the tire cornering stiffnesses that appear in the Bicycle Model equation [**5**]. The understeer gradient is shown in Eq. **1.3**. Again, tire cornering stiffnesses are negative values.

$$K_{us} = \left(\frac{W_r}{C_r} - \frac{W_f}{C_f} \right) \qquad \text{Equation } \mathbf{1.3}$$

Another important quantity is the vehicle slip angle, or sideslip angle. It is seen graphically in Fig. 1.3 as the difference between the vehicle’s instantaneous velocity vector and the longitudinal axis of the vehicle. Sideslip is defined by $\beta = V/U$, and when measured at the vehicle’s CG, can be written as shown in Eq. 1.4 [8**]**.

$$\beta = \frac{l_r}{R} + \frac{W_r}{C_r \cdot g} \frac{U^2}{R} \qquad \text{Equation } \mathbf{1.4}$$

Thesis Summary

The main goal of this work is to further existing vehicle dynamics research by developing more advanced instrumentation systems and testing additional vehicles. The remainder of this thesis will be organized as follows:

Chapter Two will discuss tire properties, their measurement, and the various factors that influence them.

Chapter Three will explain the instrumentation system that will be installed in a test vehicle. Also discussed will be the static and dynamic parameters required for analyzing the tire and chassis dynamics.

Chapter Four will present the experimental testing results in detail and combine the test data with assumptions made in the Bicycle Mode in order to calculate or approximate various vehicle and tire properties.

Chapter Five will compare the results to prior results and published data. The consistency and accuracy of the instruments and testing method will be judged.

Chapter Six will present the conclusions and recommend future work.

1. W.F. Milliken and D.L. Milliken, *Race Car Vehicle Dynamics*: Society of Automotive Engineers, 1995.

2. MTS Systems Corporation, http://www.mts.com

3. B.C. Hamblin, R.D. Martini, J.T. Cameron, and S.N. Brennan, “Low-Order Modeling of Vehicle Roll Dynamics,” *Proceedings of the 2006 American Control Conference*, 2006.

4. R.D. Martini, “GPS/INS Sensing Coordination for Vehicle State Identification and Road Grade Positioning,” *The Pennsylvania State University,* 2006.

5. D.M. Bevly, R. Sheridan, and J.C. Gerdes, “Integrating INS Sensors with GPS Velocity Measurements for Continuous Estimation of Vehicle Sideslip and Tire Cornering Stiffness,” *Proceedings of the 2001 American Control Conference*, 2001.

6. L. Segel, “Research in the Fundamentals of Automobile Control and Stability,” *Society of Automotive Engineers*, 1956.

7. R.T. Bundorf, “A Primer on Vehicle Directional Control,” *General Motors Engineering Staff Report A-2730*, 1968.

8. T.D. Gillespie, *Fundamentals of Vehicle Dynamics*: Society of Automotive Engineers, 1992

9. H.B. Pacejka, *Tire and Vehicle Dynamics, Second Edition*: Society of Automotive Engineers, 2006.

Chapter 2

Tire Properties

As discussed in the previous chapter, the lateral force developed by a tire is the product of the tire's cornering stiffness and the wheel's slip angle. However, the cornering stiffness is a variable heavily dependent on several other factors and varies widely among different tires and operating conditions. This chapter will discuss factors that influence cornering stiffness, related tire measurements, and trends as pertaining to this research.

Influences on Cornering Stiffness

While the cavity shape, construction, and tread pattern and compound of a tire all have significant effects on a tire's cornering stiffness, there are only two primary variables (aside from the tire mounting geometry) that can change the cornering stiffness of a tire once it has been designed and manufactured. These variables are vertical load and inflation pressure. In general, the cornering stiffness of a tire increases with increasing load until a saturation point is reached, after which cornering stiffness decreases with load [**1**]. Fig. **2.1** shows the concave shape of the cornering stiffness vs. load graph [**1**].

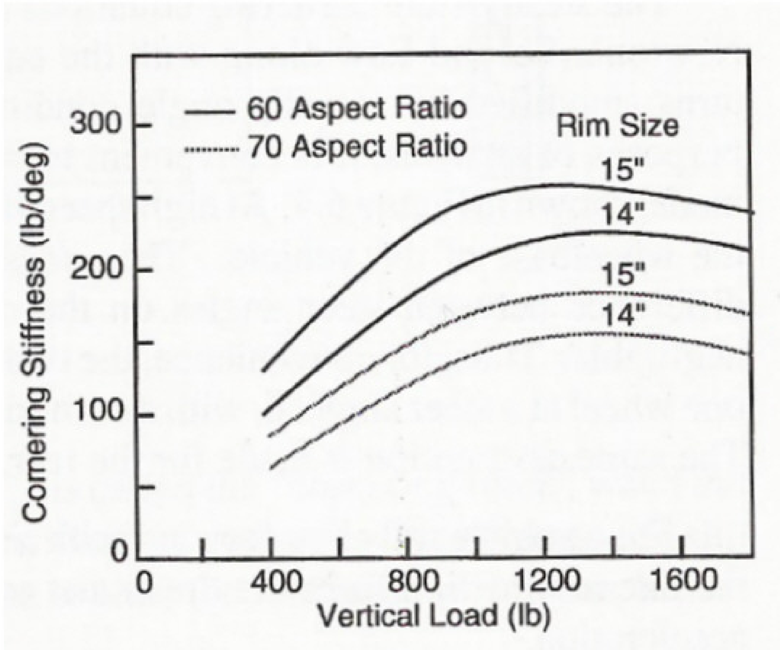

Figure **2.1**: Cornering Stiffness and Cornering Coefficient vs. Load

However, this saturation point is not usually reached until after the tire's maximum rated load has been exceeded, which is an intentionally designed feature of tires [**1**]. This situation may arise during extreme cornering maneuvers, which will not be performed during tests conducted for this study. So while it is not necessary to consider situations in which the vertical load exceeds the saturation point in this study, it is important to consider situations which increase the vertical load on the tires enough to increase the cornering stiffness. Two such foreseeable situations causing changes in vertical load include 1) changing the weight of passengers and equipment in the test vehicle, and 2) the small lateral load transfer that occurs during normal cornering. For the purposes of this study, vehicle weights will be taken with the vehicle fully loaded; however the difficulty in measuring lateral load transfer and the limitations of the Bicycle Model will necessitate that this effect is neglected.

While load plays the most important role in influencing cornering stiffness, inflation pressure is also a factor, albeit one that is even more complicated and less understood. Depending on the tire and the load conditions, increasing the inflation pressure may either increase or decrease the cornering stiffness. This is because increasing the inflation pressure increases the overall stiffness and rigidity of the tire (serving to increase cornering stiffness), while simultaneously reducing the size of the tire contact patch (reducing cornering stiffness) [**1**]. These phenomena are being studied by tire manufacturers but are beyond the scope of this paper. To ensure consistency, the inflation pressure of the tires on all vehicles will be set to the pressure specified by the vehicle manufacturer prior to testing.

Graphical Representations and Other Measurements

Graphs illustrating tire lateral force properties are commonly presented in two forms: lateral force vs. slip angle and cornering stiffness vs. load. The first method is shown in Fig. **2.2 [2]**. In this case, the slopes of the curves at zero slip angle is the cornering stiffness.

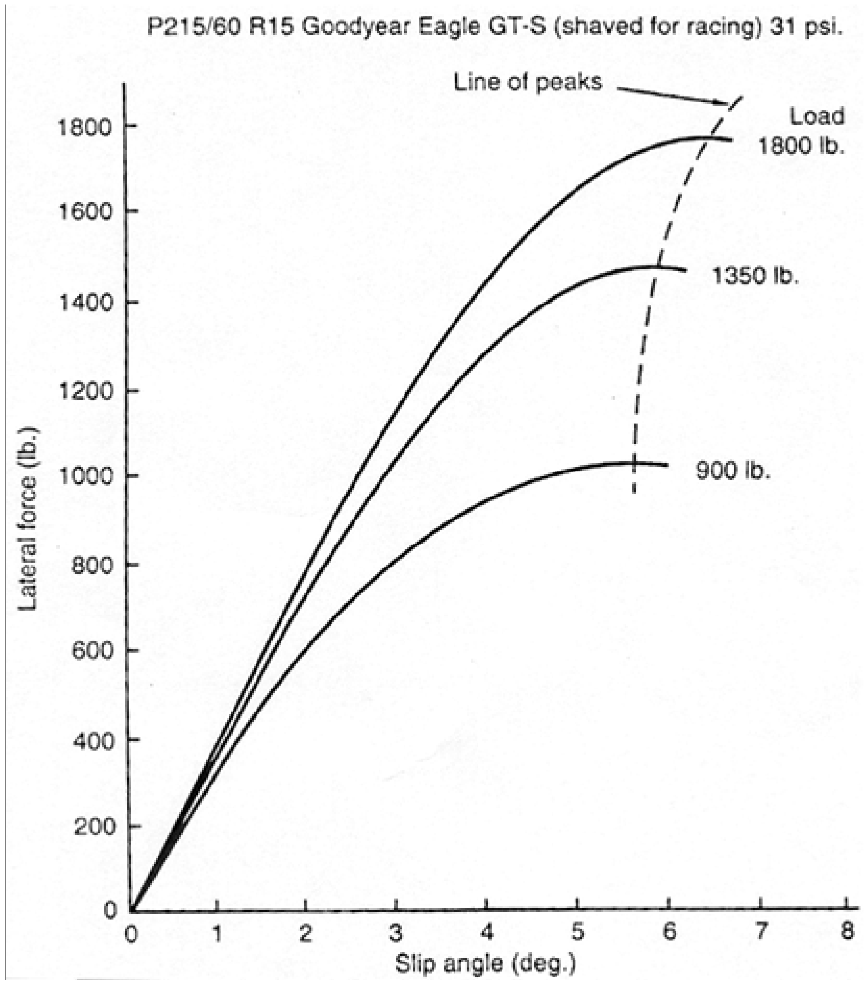

Figure **2.2**: Lateral Force vs. Slip Angle

The second graphical method is shown in Fig. **2.3** **[1]**. In this case, the slope of the curve represents the sensitivity of a tire's cornering stiffness to load changes. The technical name for this quantity is the cornering coefficient [**1**].

The cornering coefficient is important because it theoretically allows the cornering stiffness of a tire at a known load to be extrapolated to find cornering stiffness at another load. This is only applicable below the saturation load of the tire (which will not be reached during testing, as previously discussed). The cornering coefficient can be generalized for different types of tires, as shown in Fig. **2.4 [1]**. This allows trends to be analyzed between sets of similar or disparate tires.

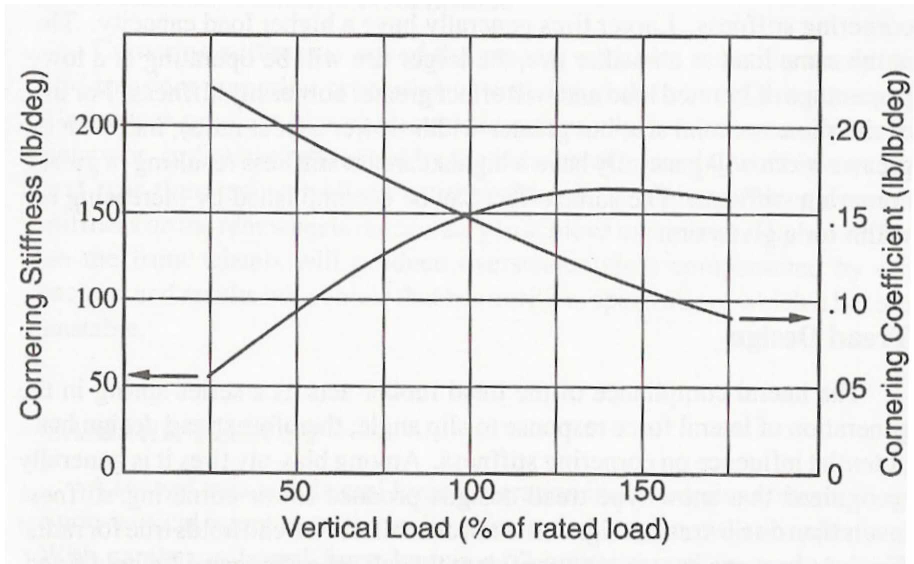

Figure **2.3**: Cornering Stiffness vs. Load

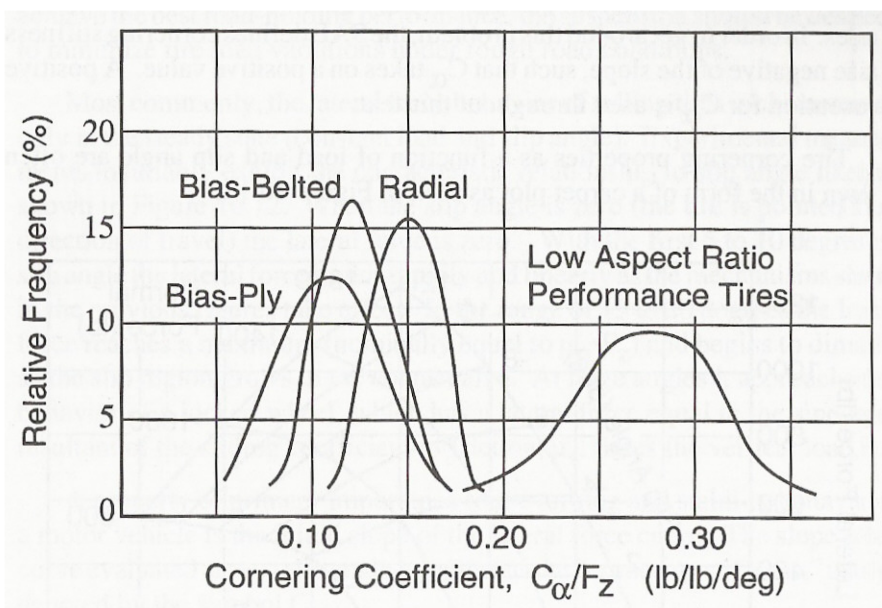

Figure **2.4**: Cornering Coefficient Ranges

Chapter Summary

Lateral forces produced by tires are equivalent to the product of the tire's cornering stiffness and the wheel slip angle. While cornering stiffness is significantly impacted by tire design, construction, and mounting, it can also be influenced by vertical load and inflation pressure, often in unpredictable ways. During testing, it is important to minimize variations in vehicle load and pressure as to obtain consistent results. Tire lateral forces can be graphed in several ways and the properties of the graphs may be used to draw generalizations about tire performance.

1. T.D. Gillespie, *Fundamentals of Vehicle Dynamics*: Society of Automotive Engineers, 1992.

2. W.F. Milliken and D.L. Milliken, *Race Car Vehicle Dynamics*: Society of Automotive Engineers, 1995.

Chapter 3

Instrumentation and Data Collection

This chapter will introduce the parameters acquired through testing as well as the methods used to obtain each parameter. Explanation of the instruments used to obtain data, including the development and calibration of new instruments, will also be presented in this chapter. The scope of this chapter will be confined to the testing methodology, while Chapter 4 will present the test results and analysis.

Static Vehicle Properties

Obtaining many of the static vehicle properties is easily accomplished by using basic measuring tools. However, the inertial parameters are extremely important and cannot be directly measured. The National Highway Transportation Safety Administration (NHTSA) has published a database of inertial parameters for select vehicles manufactured in the 1998 model year or prior [**1**]. For vehicles not included in the database, a regression technique was used, which will be detailed in this chapter. Fig. **3.1** lists the static vehicle properties, units, method of capture, and instrument.

	Static Vehicle Properties	Unit	Method	Instrument
1	Mass (corner weights)	kg	Measurement	Scales
2	Wheelbase	m	Measurement	Tape measure
3	Front track width	m	Measurement	Tape measure
4	Rear track width	m	Measurement	Tape measure
5	CG location in xy-plane	m	Calculation (1,2)	n/a
6	CG height	m	*Regression (12)	n/a
7	Yaw moment	kg-m^2	*Regression (1,2,3/4,12)	n/a
8	Pitch moment	kg-m^2	*Regression (1,2,3/4,12)	n/a
9	Roll moment	kg-m^2	*Regression (1,2,3/4,12)	n/a
10	Steering Ratio	deg/deg	Measurement	SWA sensor, slip plates
11	Understeer gradient	deg/g	Calculation	n/a
12	Roof Height	m	Measurement	Tape measure
		*Regression used in absence of NHTSA test data		

Figure **3.1**: Static Vehicle Properties

Four large analog scales were used to weigh the vehicle. This procedure yields the “corner weights” of a vehicle, which sum to the vehicle’s total mass. The measurements for the wheelbase and track widths were carefully taken with a tape measure. Using the wheelbase and the corner weights, the location of the center of gravity in the x-y plane can be calculated by using simple algebraic proportions.

The height of the center of gravity is more difficult to find. NHTSA test data exists but only for certain vehicles. A regression based on the published NHTSA data was used to approximate the CG height as a function of roof height, which is easily measured [**2**]. The regression presented in Eq. **3.1** has an R^2 value of 0.8277 and is shown graphically in Fig. **3.2** **[2]**. Units of x and Y are feet.

$$Y=0.3891x + 0.0113 \qquad \text{Equation } \mathbf{3.1}$$

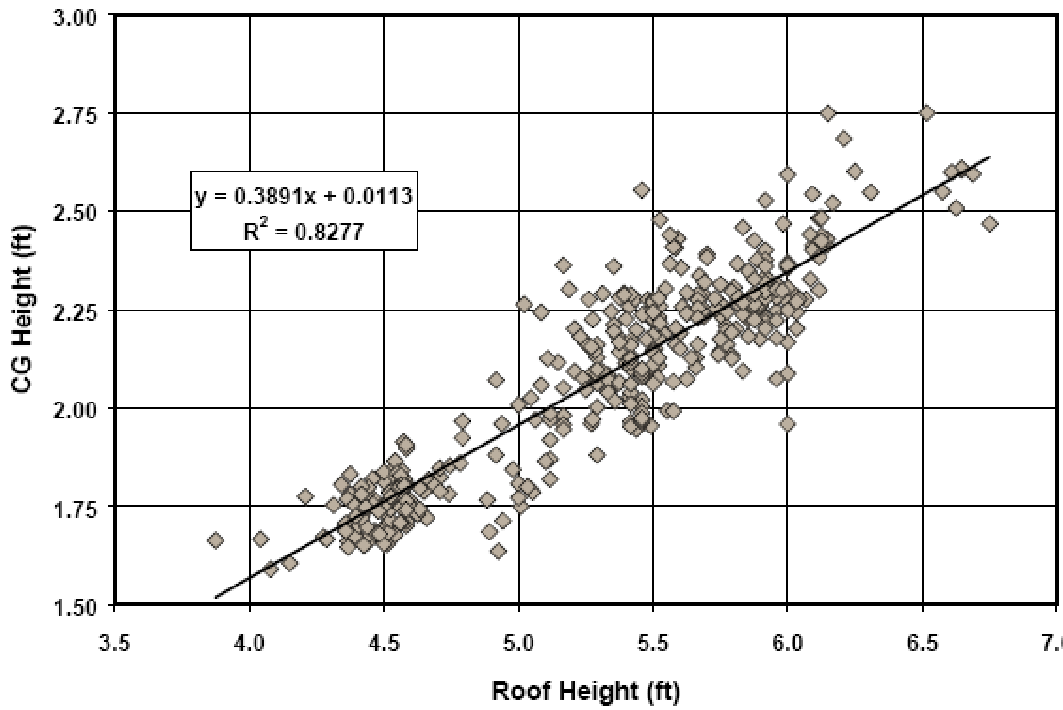

Figure **3.2**: CG Height as a Function of Roof Height

Again, NHTSA has published roll, pitch, and yaw moments of inertia but only for select vehicles. As with the CG height, a regression was used to approximate the values for vehicles with unknown inertias. Eq. **3.2** shows the general form relating the measurements of wheelbase (L, inches), track width (T_w, inches), roof height (H_r, inches) and mass (W_t, pounds) to inertia ($I_{x,y,z}$, foot-pounds-second^2). Fig. **3.3** shows the values for the regression coefficients [**2**].

$$\text{Log } I_{x,y,z} = k_1 + k_2 * \text{Log } L + k_3 * \text{Log } T_w + k_4 * \text{Log } H_r + k5 * \text{Log } W_t \qquad \text{Equation } \mathbf{3.2}$$

	roll	pitch	yaw
k1	-2.05	-1.8758	-1.6709
k2	-0.1596	1.5315	1.4316
k3	1.9404	0.2526	0.3811
k4	0.3629	0.1009	0.0188
k5	0.9421	1.0206	0.98

Figure **3.3**: Inertia Regression Coefficients

Fig. **3.4** shows the yaw regression plotted versus the actual values [**2**].

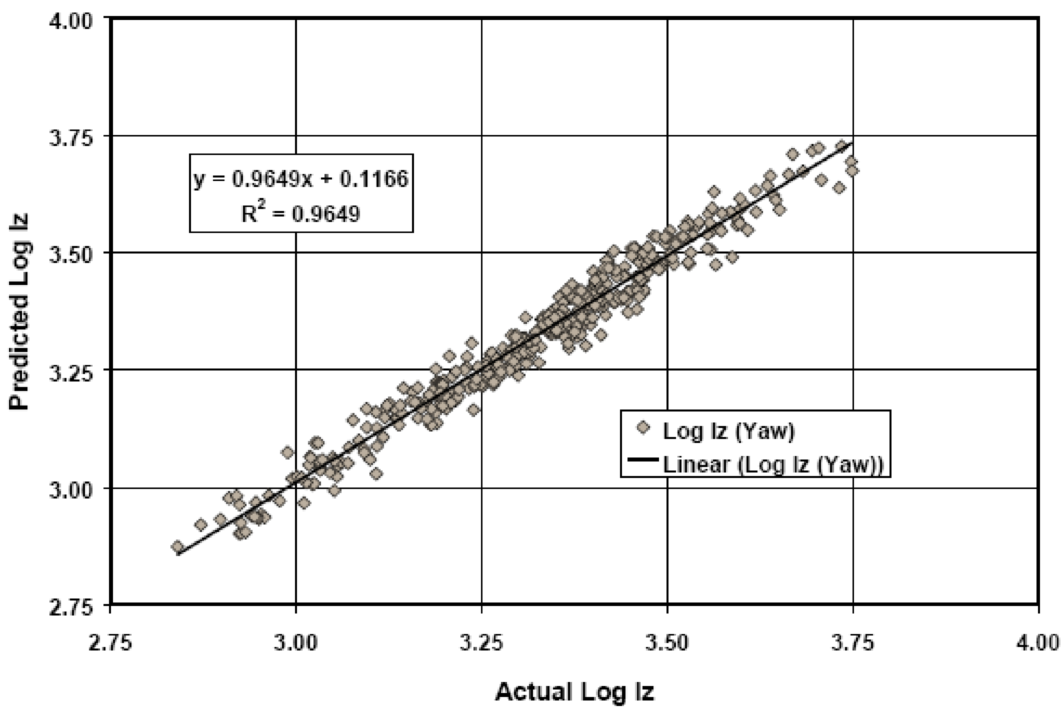

Figure **3.4**: Actual vs. Predicted Values for Yaw Moment of Inertia

To obtain the steering ratio (the ratio of the tire/wheel angle to the hand wheel angle), a steering wheel angle (SWA) sensor was used. The SWA sensor apparatus consists of a string potentiometer and a winding device. By attaching the potentiometer to the driver's side window and the winding device to the steering wheel as shown in

Fig. **3.5,** inputting a handwheel angle will tension or relax the string of the potentiometer, thus causing a measurable voltage change.

Figure **3.5**: Steering Wheel Angle Sensor

The accuracy of the SWA sensor device was checked by the use of wheel slip plates and an additional string potentiometer attached directly to the steering rack of a 1992 Mercury Tracer. By turning the steering wheel until a set angle was measured on the wheel slip plate, a set of points was obtained relating the voltage output of the steering rack potentiometer at a known roadwheel angle to the voltage output of the SWA potentiometer. Fig. **3.6** shows the steering rack angle plotted vs. the SWA sensor voltage output, which yields a very strong correlation.

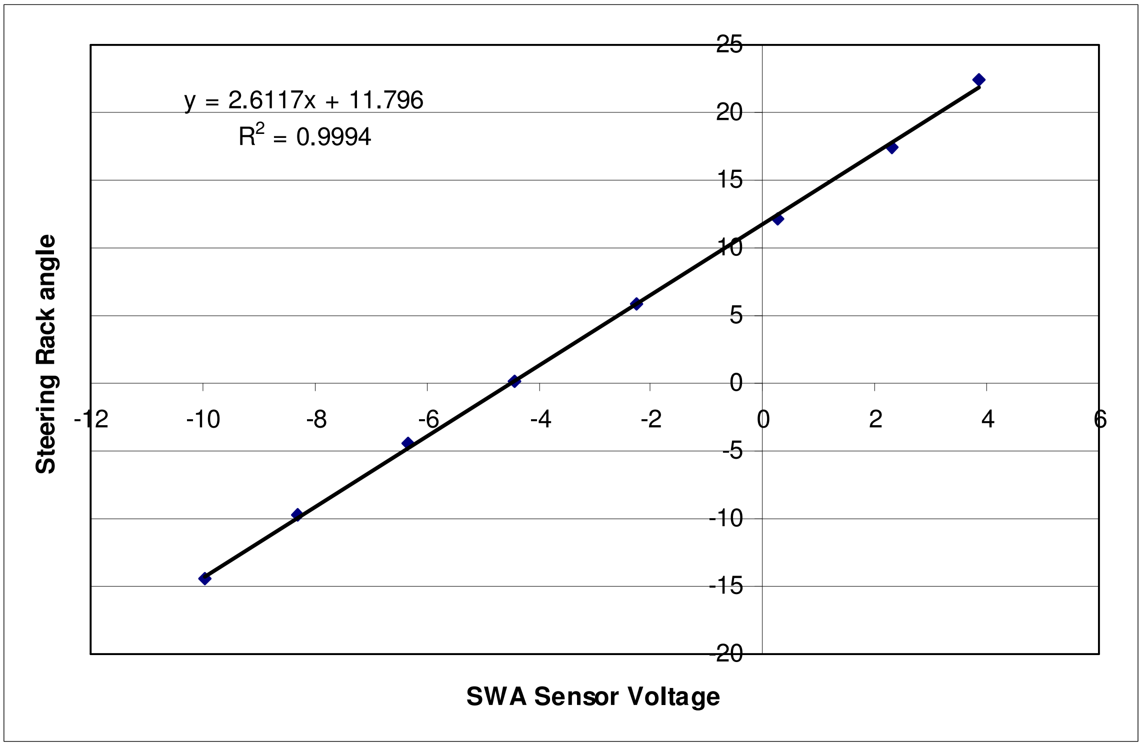

Figure **3.6**: Steering Wheel Angle Sensor Validation

To ease the process of calibrating the SWA sensor, a slip plate was equipped with two string potentiometers that could be used in conjunction with the SWA sensor to rapidly find the correlation of the SWA sensor output voltage to wheel angle. A photo of the slip plate system is shown in Fig. **3.7** and Fig. **3.8** shows the SWA sensor voltage plotted versus the output of the two slip plate string potentiometers for a maneuver in which the wheels were turned from 10 degrees left to 10 degrees right, and then back to 10 degrees left. The high degree of correlation proves that the slip plate system is accurate for use in quickly determining steering ratio.

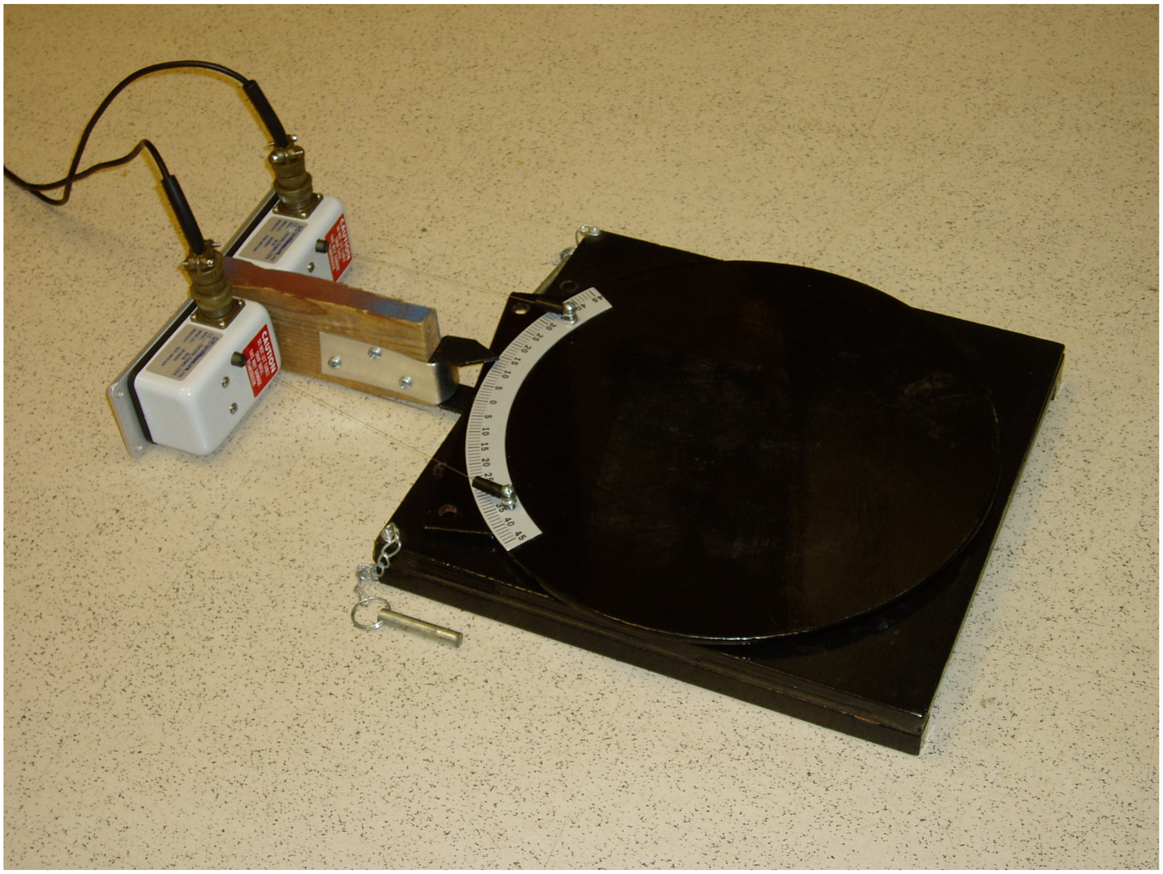

Figure **3.7**: Slip Plate With String Potentiometers

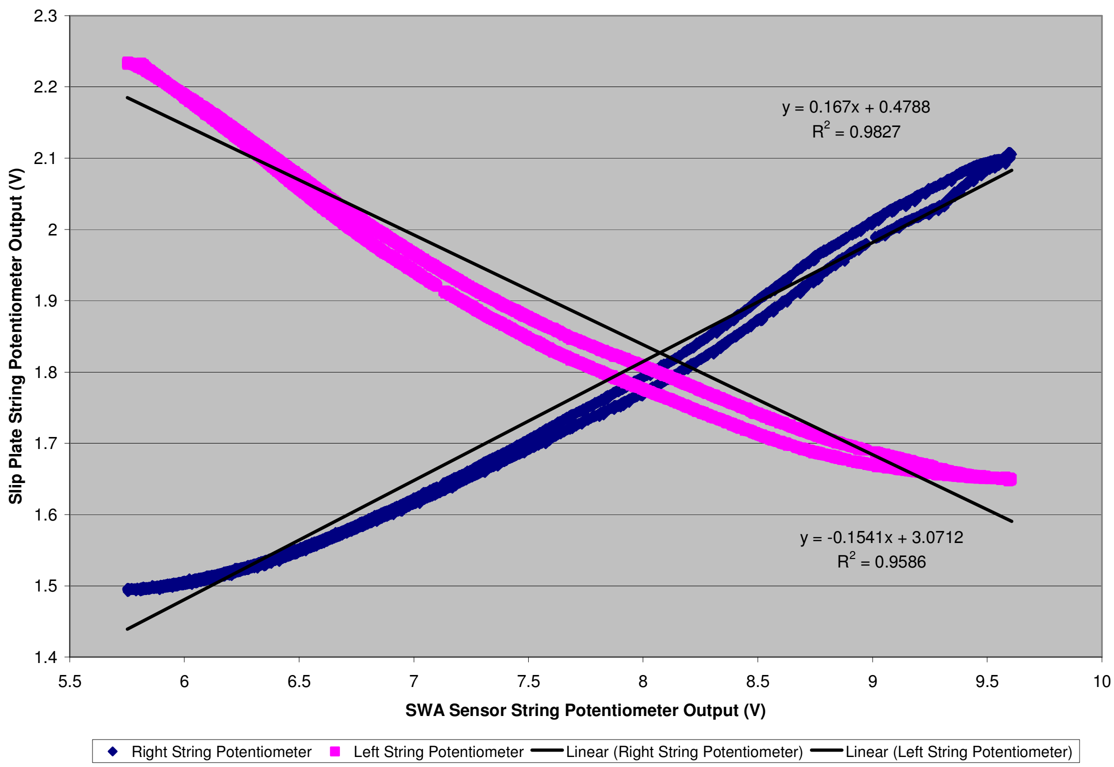

Figure **3.8**: Correlation of SWA Sensor and Slip Plate String Potentiometers

The understeer gradient is most easily obtained after dynamic maneuver data has been collected. In this case, the understeer gradient is found by using the steering angle and lateral acceleration measured while turning in a circle of known radius at several steady state velocities. In Eq. **3.3,** K is the understeer gradient [**3**]. Discussion of the dynamic parameters used in this equation will be presented in the next section.

$$\delta = 57.3*L/R + K*a_y \qquad \text{Equation } \mathbf{3.3}$$

Dynamic Vehicle Parameters

In addition to the SWA sensor already described in the previous section, the chief instrument used to capture dynamic vehicle behavior was a system combining a GPS and IMU that can provide real-time data acquisition for many parameters at a rate of 50 Hz [**4**]. The system was developed at Penn State University and had been successfully used and validated in several other previous projects [**4**] [**5**]. It was recently modified to use an Advantech xPC in place of the client CPU and DSPs used in the original system. This change was done in the interest of system performance and physical durability and was done outside of this project. Fig. **3.7** shows the setup of the GPS/IMU system in Penn State University's dedicated test vehicle and Fig. **3.8** shows the updated version of the system during testing for this work. Fig. **3.9** details the dynamic vehicle parameters, units, method of capture, and instrument. Simple geometric calculations and the North and East velocity data may be used to find the magnitude and direction of the vehicle's velocity vector.

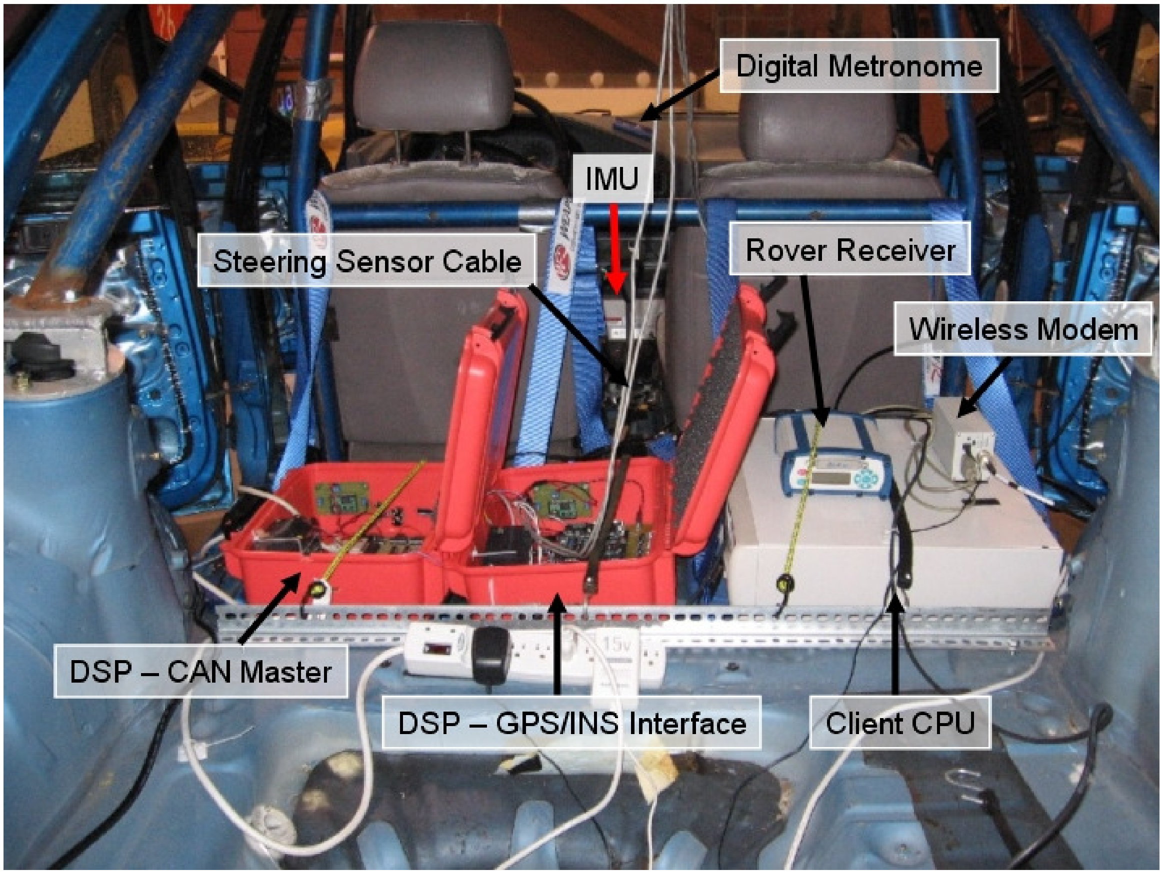

Figure **3.7**: Original GPS/IMU System Components and Setup

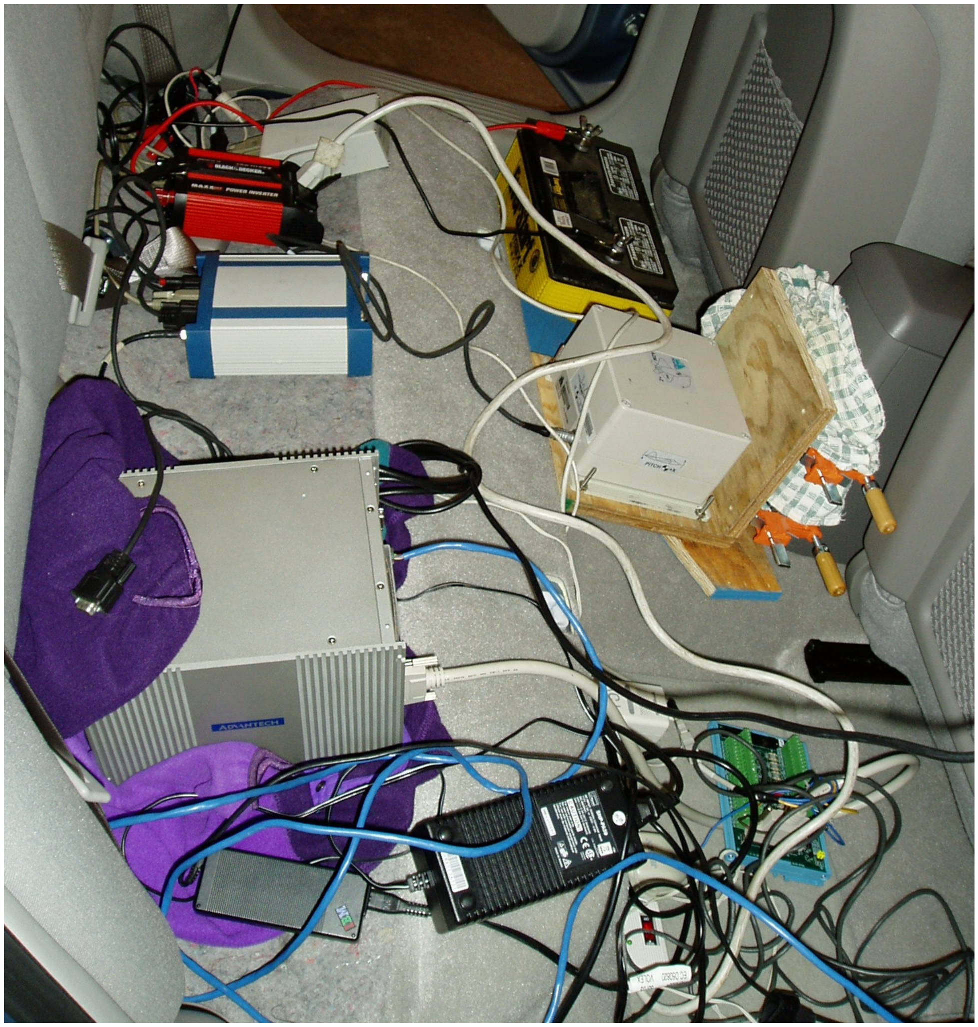

Figure **3.8**: Revised GPS/IMU System Components and Setup

	Dynamic Vehicle Parameters	Unit	Primary Method	Primary Instrument
13	North Velocity	m/s	Measurement	GPS/IMU
14	East Velocity	m/s	Measurement	GPS/IMU
15	X Acceleration	m/s^2	Measurement	GPS/IMU
16	Y Acceleration	m/s^2	Measurement	GPS/IMU
17	Z Acceleration	m/s^2	Measurement	GPS/IMU
18	Roll Angle	deg	Measurement	IMU
19	Pitch Angle	deg	Measurement	IMU
20	Yaw Angle	deg	Measurement	IMU
21	Roll Rate	deg/s	Measurement	IMU
22	Pitch Rate	deg/s	Measurement	IMU
23	Yaw Rate	deg//s	Measurement	IMU
24	Altitude	m	Measurement	GPS
25	Latitude	D-M-S	Measurement	GPS
26	Longitude	D-M-S	Measurement	GPS
27	Time	s	Measurement	GPS
28	Steering Angle	deg	Measurement	SWA sensor

Figure **3.9**: Dynamic Vehicle Parameters

1. G.J. Heydinger, R.A. Bixel, W.R. Garrott, M. Pyne, J.G. Howe, and D.A. Guenther, "Measure Vehicle Inertial Parameters – NHTSA's Data Through November 1998," *Society of Automotive Engineers*, 1999.

2. R.W. Allen, D.H. Klyde, T.J. Rosenthal, and D.M. Smith, "Estimation of Passenger Vehicle Inertial Properties and Their Effect on Stability and Handling," *Society of Automotive Engineers*, 2003.

3. T.D. Gillespie, *Fundamentals of Vehicle Dynamics*: Society of Automotive Engineers, 1992.

4. R.D. Martini, "GPS/INS Sensing Coordination for Vehicle State Identification and Road Grade Positioning," *The Pennsylvania State University*, 2006.

5. B.C. Hamblin, R.D. Martini, J.T. Cameron, and S.N. Brennan, "Low-Order Modeling of Vehicle Roll Dynamics," *Proceedings of the 2006 American Control Conference*, 2006.

Chapter 4

Vehicle Testing Results

This chapter will present the results of tests conducted on a 2007 model year Chevrolet Malibu LS four-cylinder sedan. The car was new when tested, with approximately one hundred miles on the odometer. Chapter 5 will discuss these results and compare them to results from tests of a 1992 Mercury Tracer.

Static Vehicle Properties

Mass

Weighing the Malibu with four large scales yielded the corner weight values shown in Fig. **4.1**.

Left Front	Right Front
417	399
Left Rear	Right Rear
268	240

Figure **4.1**: Measured Vehicle Corner Weights (kg)

This yielded a total mass of 1324 kg. Vehicle curb weights are readily available from a variety of sources, so the manufacturer published value for this car was compared to the measured value. According to General Motors, the mass of the vehicle is 1416 kg, with a full tank of fuel but no occupants or cargo [**1**]. The large discrepancy in the measured and published values could be attributed to the type of scales used to weigh the vehicle, which were designed for weighing extremely heavy vehicles such as trucks and buses and therefore have large increments. With no other scales available, it was decided to instead estimate the vehicle corner weights using the measured weight distribution, the manufacturer given curb weight, and an estimate of the weight of driver, passenger, and equipment.

Confidence can be expressed in this estimation because the measured fore/aft weight distribution was 61.6 % front to 38.4 % rear, which is comparable to the generally accepted distribution for most sedans, which is 60 % front and 40 % rear. This indicates that although the measured corner weights are seemingly wrong, they are in correct proportion to each other. During testing, a driver, a passenger, and testing equipment were loaded into the car, which raised the vehicle curb weight by an estimated 154 kg, bringing the total tested mass to 1570 kg. This value was scaled using the proportions of the measured corner weights to obtain the values shown in Fig. **4.2**. These values will be used for all calculations involving mass.

Left Front	Right Front
495	473
Left Rear	Right Rear
317	285

Figure **4.2**: Estimated Vehicle Corner Weights (kg)

Linear Measurements

Several important dimensional measurements were taken using a tape measure. The results, along with the manufacturer published values are given in Fig. **4.3** [**1**]. The values agree well; the measured values will be used for all further calculations.

	Measured Value	Manufacturer Value	Unit	% Deviation
Wheelbase	2.737	2.700	m	1.364
Front track width	1.537	1.524	m	0.833
Rear track width	1.505	1.506	m	0.084
Roof Height	1.429	1.461	m	2.174

Figure **4.3**: Vehicle Dimensions

Center of Gravity and Inertia

The values shown in Fig. **4.4** were obtained using the procedures outlined in the previous chapter.

	Calculated Value	Unit
CG from front axle	1.051	m
CG from rear axle	1.686	m
CG height	0.559	m
Yaw moment	2924	kg-m^2
Pitch moment	2799	kg-m^2
Roll moment	609	kg-m^2

Figure **4.4**: CG Location and Moment of Inertia Values

Although no inertial data has been published for the 2007 Chevrolet Malibu, NHTSA has published data for a vehicle that is very similar in dimension and mass, the 1998

Chevrolet Lumina sedan [**2**]. The calculated inertia values for the present test vehicle are comparable to the NHTSA published values, giving confidence to the regression used to calculate the values (see Chapter 3).

Steering System

The steering wheel angle (SWA) sensor was calibrated for the vehicle as described in Chapter 3. Fig. **4.5** shows the plot of calibration points and a linear best-fit line. Eq. **4.1** is the best fit equation that relates the output voltage of the SWA sensor (in V) to the road wheel angle (in degrees). It is important to note that the road wheel angle is measured from a line the X-Z plane and is positive by convention when the front tires are pointed so that the vehicle will travel in a clockwise direction. The R^2 value of the fit is 0.999, which is excellent correlation.

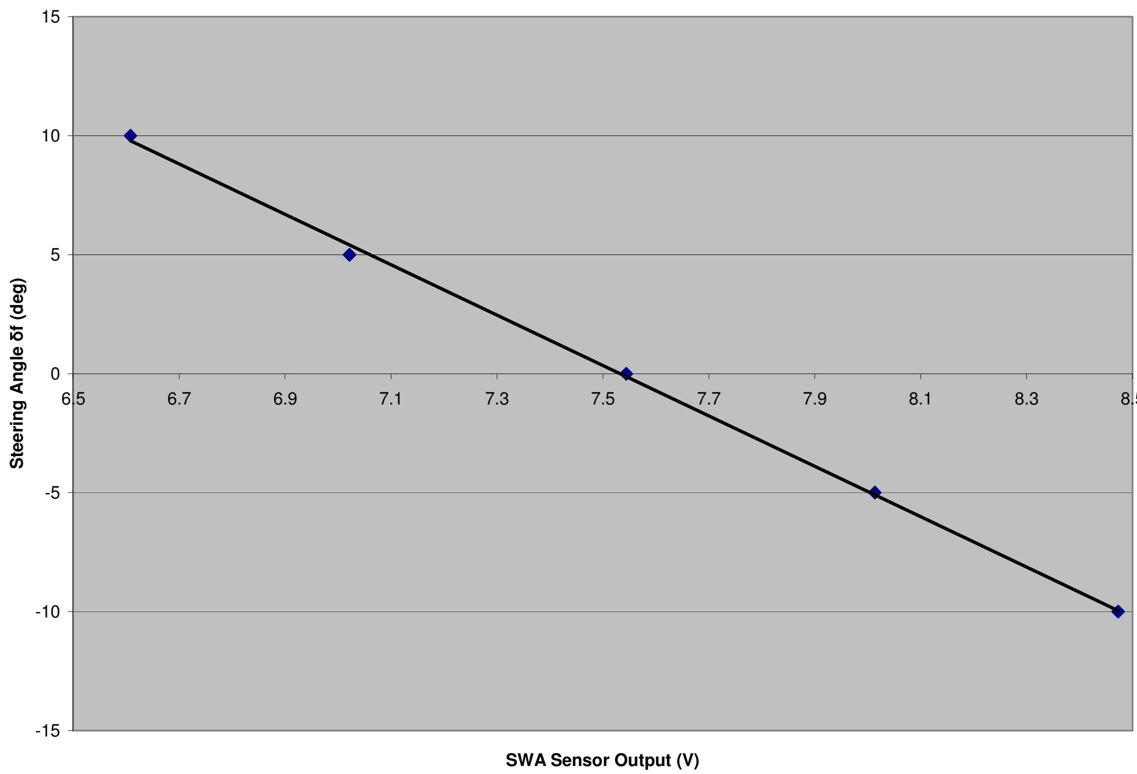

Figure **4.5**: SWA Sensor Calibration for Chevrolet Malibu

$$\delta_f = -10.579 * (SWAVoltage) + 79.685 \quad \text{Equation } \mathbf{4.1}$$

Dynamic Vehicle Testing

All dynamic vehicle testing was conducted at the Pennsylvania Transportation Institute test track located near University Park, Pennsylvania. Tests were run on the skidpad area, around a painted circle of radius 30.5 meters. Two types of tests were conducted: constant velocity and increasing velocity. In the constant velocity tests, data was recorded as the vehicle was driven both clockwise (CW) and counter-clockwise (CCW) around the circle at a steady velocity and steering input. Constant velocity tests were run at 5, 7.5, 10, 12.5, 15, 20, 25, and 30 miles per hour. For the increasing velocity tests, one run in each direction was made as the driver slowly and steadily increased velocity from 5 to 30 miles per hour. From this testing, several parameters will be found, including the understeer gradient and the rear tire cornering stiffness, which will be found by the sideslip method. The front tire cornering stiffness will be found by two different methods, the steering angle method and the understeer gradient method.

Understeer Gradient

The understeer gradient was found by plotting the average steering angle vs. the average lateral acceleration (equivalent to U^2/R) for each of the CW and CCW constant velocity circles. The slope of a best-fit line through the data is the understeer gradient. Fig. **4.6** shows this plot. Due to a data acquisition problem, the 7.5 and 12.5 mph constant velocity tests were not able to be included in this plot.

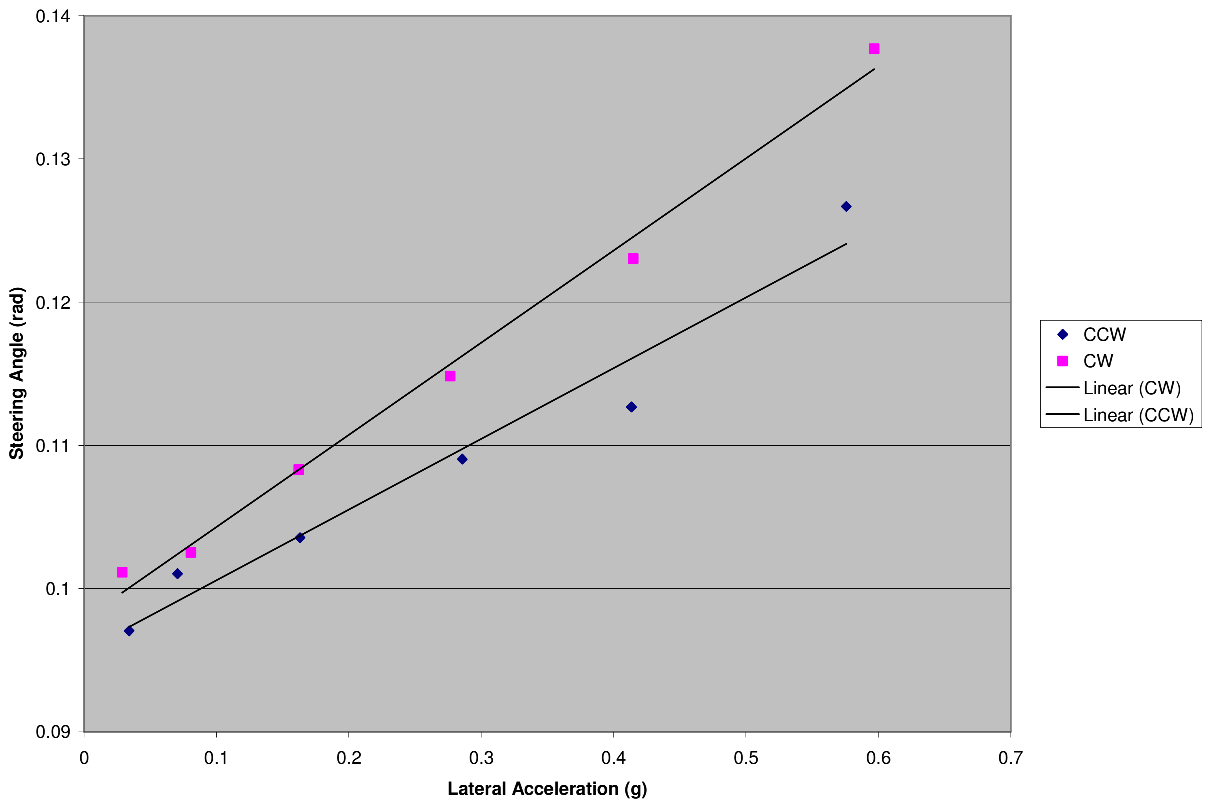

Figure **4.6**: Steering Angle vs. Lateral Acceleration

The understeer gradient for the CCW turns was 0.0494 rad/g and the understeer gradient for the CW turns was 0.0643 rad/g. The average of these values is 0.0569 rad/g, which is the value that will be used in further calculations.

Rear Tire Cornering Stiffness (Sideslip Method)

By using the data obtained during the increasing velocity tests, the Bicycle Model equations can be used to find the cornering stiffness of the rear tires. As explained in Chapter 1, sideslip is the difference between the vehicle's velocity vector and its longitudinal axis. Sideslip is defined by Eq. **4.2**.

$$\beta = \frac{l_r}{R} + \frac{W_r}{C_r \cdot g}\frac{U^2}{R}$$ Equation **4.2**

If the point where the vehicle's sideslip is zero is considered, then Eq. **4.2** can be simplified to Eq. **4.3**, which expresses the rear cornering stiffness as a function of velocity and several other easily obtained vehicle properties [**3**].

$$C_r = -\frac{W_r}{l_r \cdot g}U^2$$ Equation **4.3**

By plotting the vehicle's velocity vector and yaw angle for the tests in which the velocity was steadily increased, the time at which the zero sideslip condition occurs can be found by locating the intersection of the two curves.

Due to problems with the data acquisition system, the yaw angle was not recorded for the duration of either the CW or CCW tests. Fig. **4.7** shows the plot for the CW increasing speed test. In this plot, each period represents one complete rotation around the circle, with North corresponding to 0 degrees, East corresponding to 90 degrees, and so on. The point of intersection can be seen occurring around 75 seconds. Fig. **4.8** repeats this plot, only zoomed into the area of interest and plotted with velocity. In the CW test, the zero sideslip condition occurred at 73.56 seconds, at which time the car was traveling at 6.953 m/s. Using Eq. **4.3**, this yields Cr = -17263 N/rad.

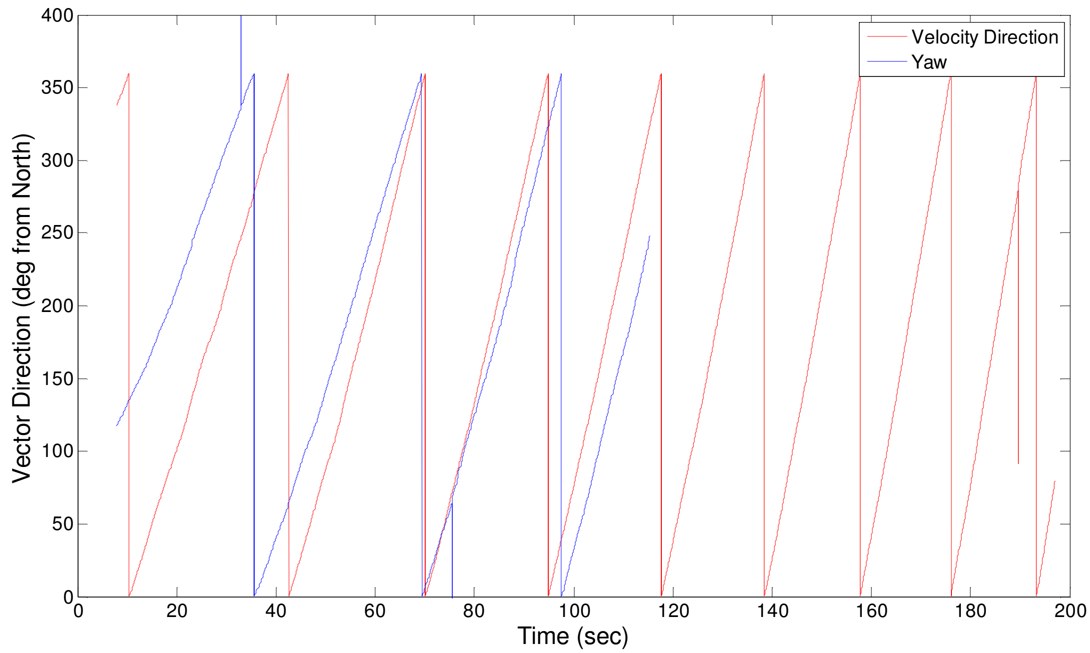

Figure **4.7**: Increasing Speed CW Vector Directions

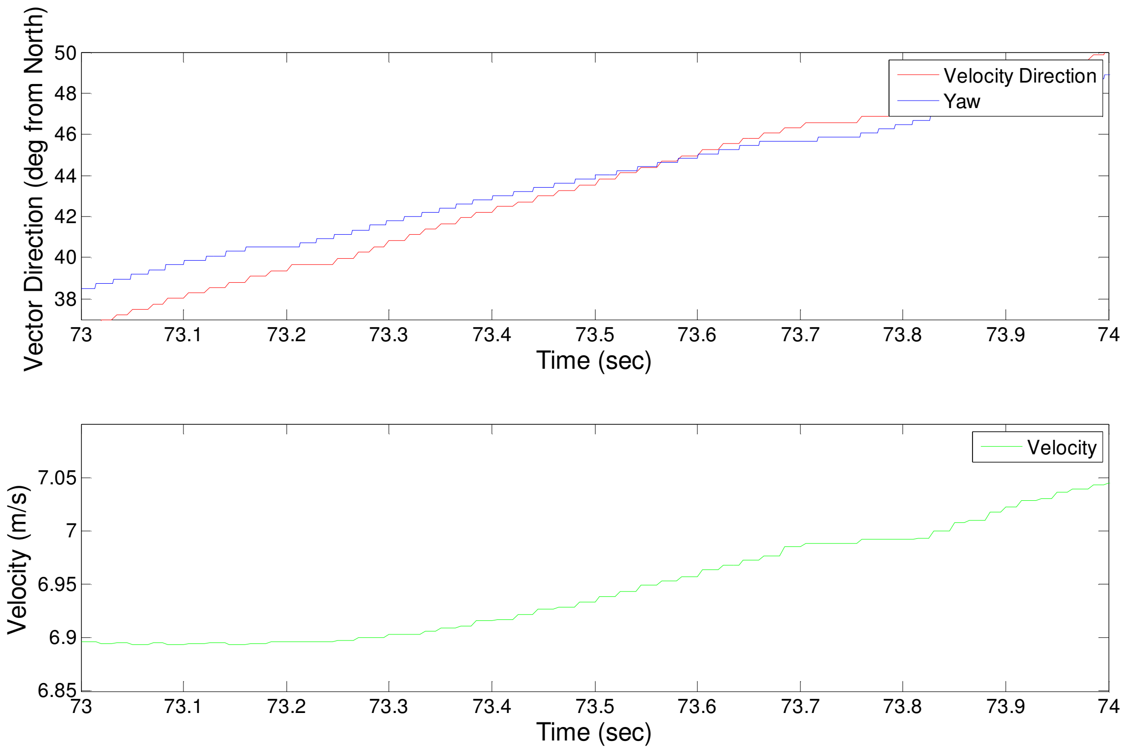

Figure **4.8**: Increasing Speed CW Vector Directions and Velocity Zoomed

Fig. **4.9** shows the plot for the CCW test. Notice that the intersection of the vectors does not occur before the recorded yaw data ends.

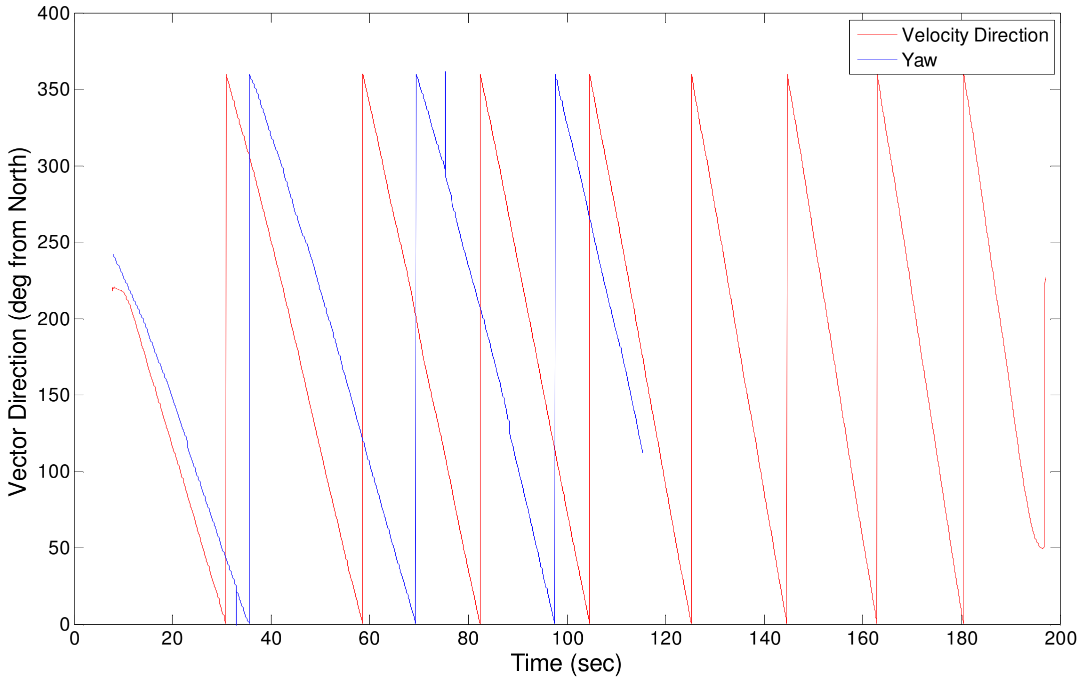

Figure **4.9**: Increasing Speed CCW Vector Directions

Fig. **4.10** displays the velocity magnitude on the same time scale as Fig. **4.9**.

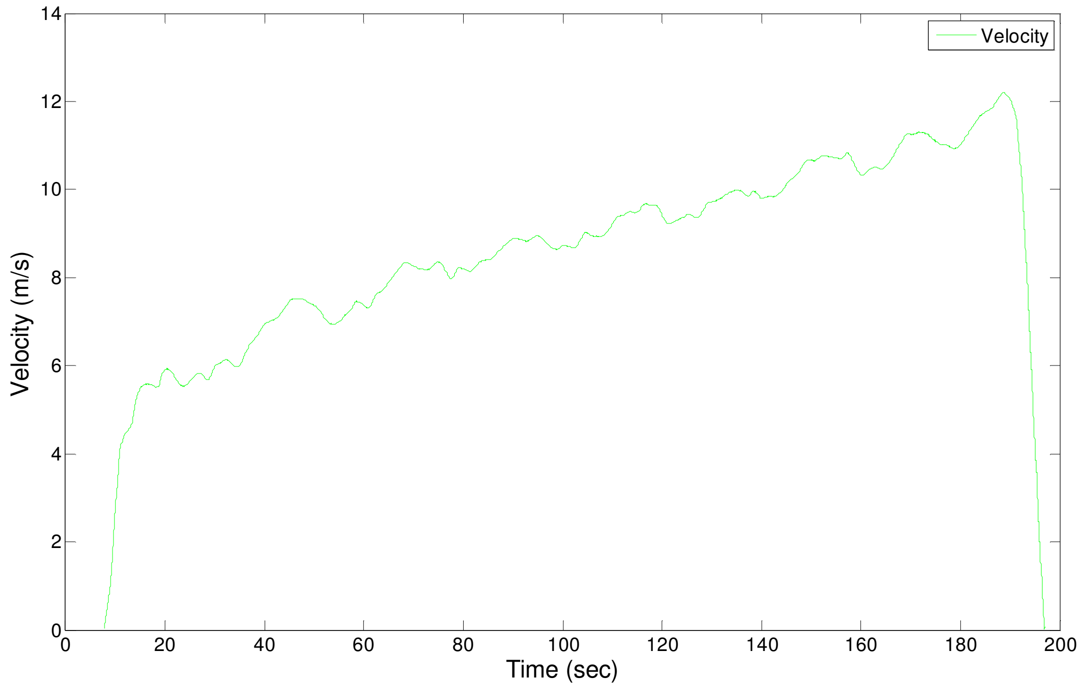

Figure **4.10**: Increasing Speed CCW Velocity Magnitude

It is evident that the velocity is increasing fairly linearly, particularly after the 100 second mark. Because the yaw velocity (rate at which the yaw angle changes) is defined as shown in Eq. **4.4**, it is dependent entirely on the velocity of the vehicle in this situation because the turn radius is constant [**4**]. Therefore, the missing yaw data can be predicted by extrapolating the existing data.

$$r = U/R \qquad \text{Equation } \mathbf{4.4}$$

Fig. **4.11** shows the results of the extrapolation. The point of intersection can be seen occurring at 125.2 seconds and 9.433 m/s.

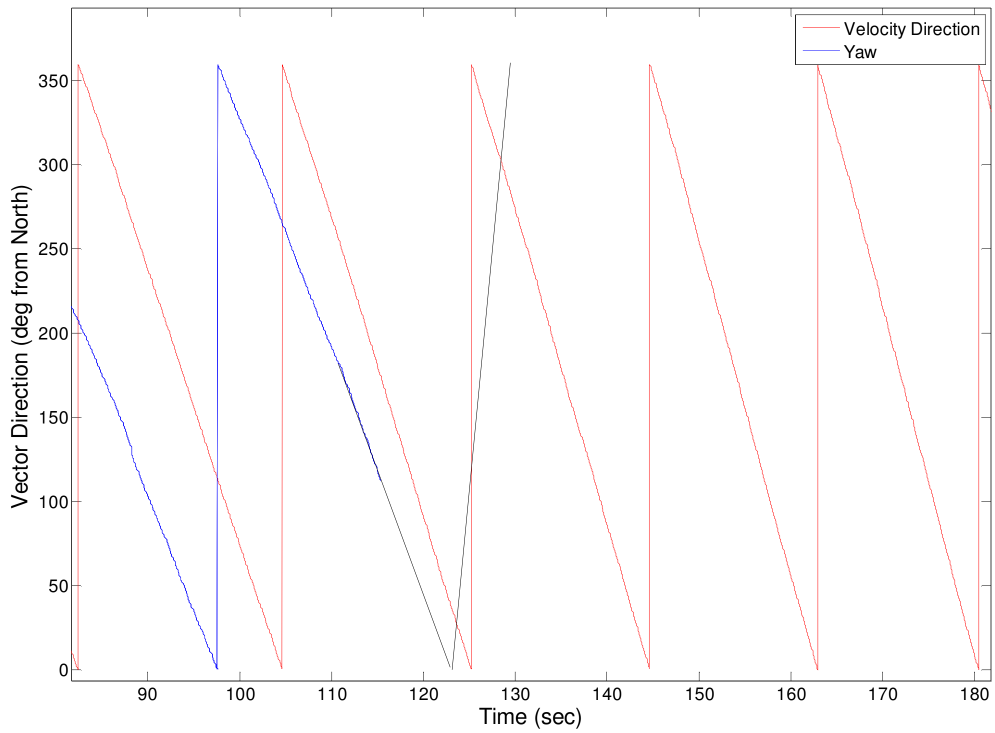

Figure **4.11**: Increasing Speed CCW Vector Directions Extrapolated and Zoomed

Eq. **4.3** gives Cr = -31774 N/rad for the CCW test.

Front Tire Cornering Stiffness (Steering Angle Method)

Recalling the Bicycle Model equation from Chapter 1 (Eq. **4.5**), it is seen that all of the variables have been capture except for the front tire cornering stiffness.

$$\delta_f = \frac{L}{R} + \left(\frac{W_r}{C_r} - \frac{W_f}{C_f} \right) \frac{U^2}{g \cdot R} \qquad \text{Equation } \mathbf{4.5}$$

By rearranging the terms as in Eq. **4.6**, Cf is readily solved. Eq. **4.1** is used to find the steering angles, which are 0.1034 rad for the CW test and 0.1090 rad for the CCW test. The Cf values are -22234 N/rad for the CW circle and -37870 N/rad for the CCW circle.

$$C_f = \frac{-W_f}{\left(\delta_f - \frac{L}{R}\right)\frac{g \cdot R}{U^2} + \frac{W_r}{C_r}}$$ Equation **4.6**

Front Tire Cornering Stiffness (Understeer Gradient Method)

The understeer gradient can also be used to solve for Cf [3]. By rewriting the definition of the understeer gradient (Eq. 4.7) as Eq. 4.8**,** Cf may be easily calculated. Using the Kus = 0.0569 as calculated earlier in this chapter, the Cf for the CW test is found to be -23795 N/rad and the Cf for the CCW test is found to be -39105 N/rad.

$$K_{us} = \left(\frac{W_r}{C_r} - \frac{W_f}{C_f}\right)$$ Equation **4.7**

$$C_f = \frac{W_f \cdot C_r}{W_r - C_r \cdot K_{us}}$$ Equation **4.8**

Chapter Summary

In this chapter, static vehicle properties of a 2007 Chevrolet Malibu test car were presented. Using this information and results from constant velocity circle tests and increasing velocity circle tests, chassis and tire properties such as the understeer gradient and tire cornering stiffnesses were calculated in various ways. Chapter 5 will focus on discussing these results, citing possible sources of error, and comparing to previous test results.

1. General Motors, http://www.gm.com

2. G.J. Heydinger, R.A. Bixel, W.R. Garrott, M. Pyne, J.G. Howe, and D.A. Guenther, “Measure Vehicle Inertial Parameters – NHTSA’s Data Through November 1998,” *Society of Automotive Engineers*, 1999.

3. B.C. Hamblin, R.D. Martini, J.T. Cameron, and S.N. Brennan, “Low-Order Modeling of Vehicle Roll Dynamics,” *Proceedings of the 2006 American Control Conference*, 2006.

4. T.D. Gillespie, *Fundamentals of Vehicle Dynamics*: Society of Automotive Engineers, 1992.

Chapter 5

Discussion and Comparisons

While the previous chapter presented calculated values for the understeer gradient and tire cornering stiffnesses of a 2007 Chevrolet Malibu, the question remains if these values are accurate and consistent with previous test results. This chapter will address these questions as well as explore possible sources of error and shortfalls of the testing method.

Understeer Gradient

In the current study, the disparity between the understeer gradient calculated for the CCW circles and the CW circles is very apparent. The understeer gradient for the CCW turns was 0.0494 rad/g and the understeer gradient for the CW turns was 0.0643 rad/g, with an average 0.0569 rad/g. While there is variation between the understeer gradient in the two directions, it may be a result of the properties of the vehicle and not the result of testing error. Consider Fig. **5.1,** which depicts the sums of the left and ride side masses corner weights. 51.7% of the Malibu's weight rests on its left side tires. Lateral load transfer to the left wheels from the CW turn will exaggerate this static lateral CG offset and, because there is less weight on the inside wheels, their ability to generate lateral force will be reduced, causing the vehicle to understeer [**1**]. If the vehicle is turning in the opposite direction (CCW) then the reverse occurs, and the car's weight is more evenly balanced, leading to less understeer. This concept is very important in automobile racing but substantially less important to the drivers of passenger vehicles, who are unlikely to notice these slight differences in turning performance.

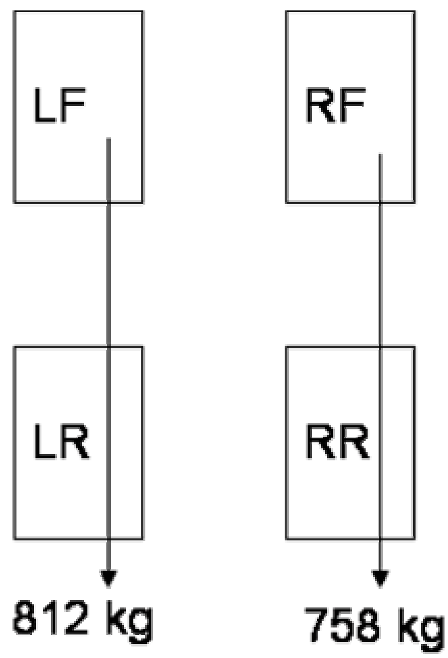

Figure **5.1**: Lateral Weight Distribution

In previous research conducted on a 1992 Mercury Tracer station wagon, the same method was used to obtain the understeer gradient, which was 0.016 rad/g for both CW and CCW directions [**2**]. While the understeer gradient of the Malibu is substantially higher, it is still less than a published sample value [**1**]. That unknown vehicle's understeer gradient was 0.0733 rad/g. Anecdotal and speculative evidence also supports that the understeer gradient of the Malibu should be larger than the understeer gradient of the Tracer. The same driver performed tests on both vehicles and remarked that the Tracer was physically easier to drive around the skidpad circle at speeds greater than 20 miles per hour, and the Malibu was not even able to exceed 30 miles per hour, while the Tracer was able to reach 35 mph.

Cornering Stiffness

There is a large difference between the cornering stiffness values calculated for the CCW increasing speed test and the values calculated from the CW increasing speed test. A summary of the cornering stiffness values is shown in Fig. **5.2**.

Quantity	CW Direction Tests	CCW Direction Tests	Average	Unit
Cr (Sideslip method)	-17263	-31744	-24504	N/rad
Cf (δf method)	-22234	-37870	-30052	N/rad
Cf (Kus method)	-23795	-39105	-31450	N/rad

Figure **5.2**: Summary of Calculated Cornering Stiffnesses

Comparisons

Intuition suggests that the lower CW cornering stiffness values are the result of a data anomaly, although the higher CCW values have uncertainty because they were calculated from a regression on the yaw data. All of the values become suspect when compared to values from other sources. During the tests of the Mercury Tracer, the Cr (Sideslip method) of that vehicle was determined to be -49300 N/rad, the Cf (δf method) was -57700 N/rad, and the Cf (Kus method) was -68400 N/rad [**2**]. All of these values are higher than the ones obtained during the current study, despite the fact that the Tracer is a lighter vehicle. As discussed in Chapter 2, a lighter load on a tire would likely lower the cornering stiffness values. Very little cornering stiffness data from tire testing machines is publicly available; however data for a set of five racing tires is available. The cornering stiffnesses range from -97550 N/rad at 816 kg for an amateur race tire to -190985 N/rad at 453 kg for a Formula 1 race car tire [**1**]. This author's personal knowledge gained from experience as an engineer at a tire manufacturing company also suggests that the values are lower than would be expected for tires on a vehicle such as the Chevrolet. For all of these reasons, it can be concluded that the cornering stiffnesses calculated during this research are very likely inaccurate.

Cornering Coefficient

While cornering stiffness is an important variable, the cornering coefficient (or load sensitivity) of a tire is also important. The cornering coefficient was defined in chapter 2 and Fig. **2.4** showed ranges of typical values. As the tires mounted on both the Tracer and the Malibu are modern performance tires, the expected value of the cornering coefficient should be between 0.25 and 0.30. Fig. **5.3** shows the cornering stiffness values for all of the cases graphed vs. the normal load. Also displayed are the cornering coefficient (CC) values for each case. For ease of comparison, the negative of the cornering stiffness values have been plotted and the CC values are in units of lbs./lbs./deg and have been doubled to represent what the load sensitivity of a single tire would be.

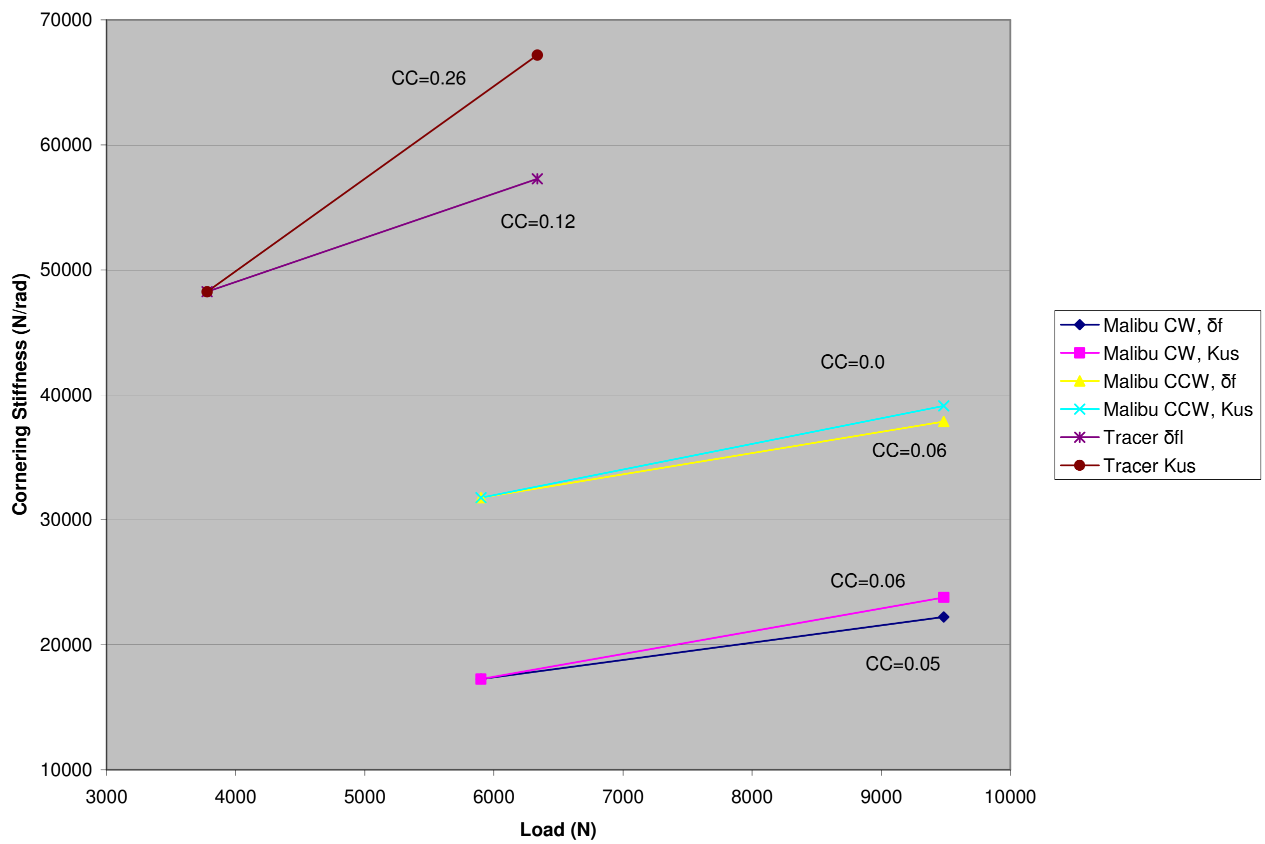

Figure **5.3**: Cornering Stiffness vs. Load

Of all the cases, only the Tracer, calculated with the Kus method, has a cornering coefficient value in the expected range. Also, the cornering coefficient values found in the current research are exceptionally well below the expected values. This is further evidence that the testing method seems to incorrectly predict cornering stiffness values.

Possible Sources of Error

The main and inherent limitation of determining cornering stiffness and understeer gradient using the Bicycle Model is the list of assumptions necessary to use the model and the practical limitations of measuring certain parameters. Nearly all of the influences that could introduce error into the understeer gradient and cornering stiffness are found in what is known as the understeer budget, which is a tabulation of the components that add together to form the understeer gradient [**1**]. Some of items included in the understeer budget are tire cornering stiffness (which is the largest contributor), camber effects, roll steer, steering system lateral force compliance, tire aligning torque, and lateral load transfer effects [**3**].

Many of these parameters are unaccounted for in this research. Although the Bicycle Model accounts for steering introduced by roll steer, camber steer, and steering system compliance, these effects are very difficult to measure practically. Therefore, they have been neglected here. The Bicycle Model assumes that effects due to lateral load transfer are limited, so it has been neglected as well. Because the Chevrolet was brand new when tested, it can be assumed that the suspension and steering systems are tight and undamaged by wear; compliance will likely increase as the vehicle ages but may exist even when the vehicle is new. Therefore, if these effects, at the lowest levels they will be over the life of the vehicle, are indeed causing the errors in cornering stiffness, they should be considered significant.

It is obvious that a vehicle has many factors influencing the understeer gradient, and in turn the tire cornering stiffness. However a tire testing machine does not have these effects. Therefore, it may be impossible to compare cornering stiffness found from vehicle testing to cornering stiffness found from tire machine testing. However, comparing cornering stiffnesses between different vehicles, provided that they have been tested using the same method and assumptions, may be possible.

1. W.F. Milliken and D.L. Milliken, *Race Car Vehicle Dynamics*: Society of Automotive Engineers, 1995.

2. B.C. Hamblin, R.D. Martini, J.T. Cameron, and S.N. Brennan, "Low-Order Modeling of Vehicle Roll Dynamics," *Proceedings of the 2006 American Control Conference*, 2006.

3. T.D. Gillespie, *Fundamentals of Vehicle Dynamics*: Society of Automotive Engineers, 1992

Chapter 6

Conclusion

One of the most important decisions in vehicle dynamics research is choosing a model. In this research, the 2-DOF Bicycle Model was chosen for its simplicity and proven accuracy. Most models have assumptions or limitations, and the Bicycle Model is not an exception. The Bicycle Model assumptions permitted convenient ways to solve for several key quantities, such as vehicle understeer gradient and tire cornering stiffness. By observing special test conditions, such as zero sideslip, the rear cornering stiffness could be mathematically isolated and solved. Tire cornering stiffness is an essential parameter for use in vehicle dynamics modeling and research; however there is very little published data. A simple and reliable method of obtaining it would help promote vehicle dynamics research in academia.

The integration of a GPS system and an INS system has been proven to be a reliable method of logging vehicle motion. Used in conjunction with the steering wheel angle sensor and wheel slip plate sensors, all of the critical inputs to the Bicycle Model can be captured, as they were when a 2007 Chevrolet Malibu was instrumented and tested.

The understeer gradient and tire cornering stiffness obtained for the Chevrolet were compared to published sample values and previous test data. The understeer gradient fell within the expected range. However, the tire cornering stiffnesses were significantly lower than expected. The sources of this error are likely the several effects that contribute the understeer budget that are neglected in the Bicycle Model or that were not measure due to physical measurement difficulties. After considering these effects, it was concluded that it may not be possible to compare the cornering stiffness of tires mounted on an actual vehicle to the cornering stiffness of tires tested using a machine. This is an important finding, as it is generally assumed or implied in research that the two sets of data are interchangeable.

Future research may include the testing of more vehicles using the same methods or may focus on other methods to obtain cornering stiffness, such as frequency response maneuvers. Higher order models may also need to be considered if a way to measure steering and suspension effects is not developed. Regardless of the type of testing or model, the refinement of GPS/INS systems should continue, given the promising results that have been obtained during vehicle testing and the wide range of applications of such systems. However, determining the validity of any experimental method requires collecting many data sets to ascertain accuracy and precision, and currently there have not been enough tests conducted to make firm conclusions. If a simple method of obtaining tire and chassis dynamic parameters is found, it will lead academia to a greater understanding of vehicle behavior, which could translate into safer vehicles, autonomous vehicles, or other applications.